Journal of Science and Technology, 4(1): 38-50, 2025
DOI: 10.69560/cujast.1618074

Journal of Science and Technology

| cujast.cumhuriyet.edu.tr | Founded: 2025 Available online, ISSN: 2980-0110 Publisher: Sivas Cumhuriyet Üniversitesi

Strain Effect and Artificial Intelligence Applications on Electronic Band Structure of MoS_2

Hamdi Dağıstanlı[1,a,*]

[1] *Konak Radikal Anatolian High School, İzmir, Türkiye*
**Corresponding author*

Research Article

History

Received: 11/01/2025
Accepted: 24/02/2025

ABSTRACT

Ab initio density functional theory (DFT) calculations have been utilised to ascertain the band gap of the 2D layered material MoS_2 under uniaxial strain. This involves finding optimised lattice parameters and calculating the electronic band structure. It is also noted that by applying strains ranging from -15% to 15%, a wide range of band gaps can be obtained to study the behaviours of the semimetal and metal. The ensuing outcomes are then applied to the domain of machine learning. Initially, PR, which is polynomial regression, is a machine learning method that can be studied with numpy, sklearn and scipy modules, and ANN (artificial neural network) is the application with tensorflow module that is applied to the optimised semi-metallic and metallic structures. The application of the latter involves the Least Squares method. The implementation of Leaky Relu (LRelu) and Elu functions is instrumental in facilitating the deployment of ANN. The potential dataset is obtained by using Quantum Espresso, and the calculations are made by using the National Center for High Performance Computing of Turkey (UYBHM). The PR and ANN results are calculated using the existing data set. The primary objective of utilising PR and artificial neural networks is to facilitate the plotting of Valance Band Maximum (VBM) and Conduction Band Minimum (CBM) graphs in the vicinity of the Fermi level.
This study based on data which are already available and could therefore be considered to be data mining. on the electronic band structure for MoS_2.

Keywords: MoS_2, DFT, electronic structure, strain effect, artificial neural network, polynomial regression.

[a] *hamdi.dagistanli@gmail.com* *0000-0002-9845-9156*

How to Cite: Dağıstanlı H., (2025) Strain Effect and Artificial Intelligence Applications on Electronic Band Structure of MoS_2, *Journal of Science and Technology, 4(1): 38-50*

Introduction

Two-dimensional (2D) materials, particularly transition metal dichalcogenides (2D-TMDs), have attracted significant attention due to their remarkable electronic, optical, and mechanical properties. The chemical formula for these materials is typically MX_2, where M represents a transition metal (e.g., Mo, W, Ti, Zr, V, Nb, Pd, Pt) and X is a chalcogen (S, Se, Te) or oxygen (O). This diversity in their composition leads to a wide range of functionalities. Among the TMD family, molybdenum disulfide (MoS_2) has emerged as a benchmark material, celebrated for its semiconducting nature, high mechanical strength, and flexibility. Structurally, MoS_2 comprises layers of molybdenum atoms covalently bonded to sulfur atoms, forming a sandwich-like arrangement. These layers are held together by weak van der Waals forces, enabling straightforward exfoliation into monolayer or few-layer forms (Novoselov et al.(2004)).

MoS_2 exhibits a transition from an indirect bandgap of approximately 1.2 eV in its bulk form to a direct bandgap of around 1.8 eV when reduced to a monolayer. This property renders it an exceptionally versatile material for a wide range of optoelectronic applications (Splendiani, A., et al.(2010)). The tunability of this bandgap, in conjunction with its high carrier mobility and strong light-matter interactions, has facilitated the integration of MoS_2 into various applications, including transistors, photodetectors, and energy storage devices (Wang, Q. H., et al. (2012)).

Beyond its applications in electronics, MoS_2 demonstrates remarkable catalytic activity for hydrogen evolution reactions (HER), a critical process in renewable energy technologies (Chhowalla, M., et al. (2013)). Its unique two-dimensional (2D) structure and inherent defects significantly enhance its catalytic performance. Moreover, its mechanical durability and chemical stability position it as an excellent candidate for wearable electronics and flexible devices (Bertolazzi, S., Brivio, J. & Kis, A. (2011)).

Advances in scalable synthesis techniques, such as liquid-phase exfoliation, have led to significant expansion in the practical utility of MoS_2 (Zhan, Y., et al. (2012)). However, challenges persist, including the need for precise control of

defect density, the achievement of uniform synthesis, and the deepening of understanding of interfacial properties. These challenges continue to drive research in this field.

In the section of this article devoted to artificial intelligence, the focus is not on solving equations representing physical problems. This study can be regarded as a data mining effort focused on the electronic properties of MoS_2. The dataset is utilised as training data for electronic band calculations of MoS_2, encompassing its semiconductor, semi-metallic, and metallic behaviours. These calculations are performed using Quantum Espresso (Giannozzi, P., et al. (2009), Giannozzi, P., et al. (2020)) and National Center for High Performance Computing of Turkey (UYBHM).

The Polynomial Regression (PR) algorithm is predicted on the least squares method in order to establish a regression relationship fitted to dataset. In this study, the PR algorithm is implemented using the Python programming language, leveraging modules such as NumPy, SciPy, and scikit-learn (sklearn) (Türeci, R. G. (2022)).

Artificial Neural Networks (ANN) represent a sophisticated form of the Logistic Regression (LR) algorithm, which gives binary outcomes (true or false). In contrast to LR, ANN incorporates hyperparameters that depend on both the dataset and the expertise of the programmer. In this study, the hyperparameters that are considered include epoch, number of neurons, test size, validation split, and batch size, all of which are crucial for optimising model performance. The selection of these hyperparameters is informed by prior experience with the data.

The process of data transmission through sequential layers, commencing from the input layer and culminating in the output layer, is designated as forward propagation. Upon reaching the output layer, a comparison is made between the data and the test data, resulting in the calculation of an error value. Within the domain of machine learning, this error is designated as 'loss'. The data is then sent back to the input layer using the back propagation algorithm, based on the loss value obtained. This completes one cycle, and the number of cycles is termed an epoch. The number of epochs is thus a measure of iteration.

The activation function plays a crucial role in ensuring the transmission of data from one neuron in a hidden layer to the neuron in the subsequent hidden layer. The activation function is therefore pivotal in triggering the subsequent neuron. In this study, the Elu and ReLu activation functions (Xu, B., et al. (2015)) are employed.

It is imperative that the activation function is differentiable, since the back propagation algorithm is initiated following the calculation of the loss value, thereby activating the optimiser. The Adam optimizer (Kingma, D. P., Ba, J. L. (2017)) is utilised to optimise the coefficients from neuron to neuron employing the gradient descent method. The Adam optimizer has become the most prevalent and successful optimizer function in contemporary research.

The objective of this study is to utilise a MoS_2 structure under strain effects and to apply artificial intelligence to MoS_2, optimised, semi-metal, and metallic states.

The discussion will encompass the potential applications of artificial intelligence in MoS_2 and the advantages thereof. Following the conclusion of this study, the intention is to apply artificial intelligence to other TMDs.

The structure of the paper is as follows: in the Materials and Methods section, the methods and parameters used in the DFT and PR calculations are outlined, including Elu and LRelu. The Results section determines the atomic structure and lattice constant of MoS_2 via total energy optimization. In the same section, the density of states is calculated and artificial intelligence is applied for optimised, semi-metal and metallic states. Energy band graphics are rendered using QE, while VBM and CBM graphics are produced using PR, Elu and LRelu for optimised, semi-metal and metallic states. The results pertaining to the calculations and artificial intelligence are presented. Finally, the conclusions are presented.

Materials and Methods

Firstly, a detailed analysis of the two-dimensional (2D) hexagonal structure of MoS_2 is presented with the aim of achieving an optimal honeycomb geometry. To this end, Density Functional Theory (DFT) calculations were performed employing the Perdew-Burke-Ernzerhof (PBE) generalised gradient approximation exchange-correlation functional (Perdew, P. J., Burke, K. & Ernzerhof, M. (1996)). With an energy cutoff of 350 eV, the Projector Augmented-Wave (PAW) method (Kresse, G. (1999)) was employed.

The conjugate gradient method was used to optimise the geometry on a fully relaxed unit cell containing two atoms. Vacuum layers were introduced to ensure a separation of 10 Å to avoid interactions through the plate thickness, and normal boundary conditions were applied in all directions. To evaluate the mechanical properties and calculate the electronic density of states, sampling from the Brillouin zone was performed using a 12×12×1 k-point grid. The Monkhorst-Pack grid with a 12×12×1 k-point configuration was utilised to ensure the attainment of accurate results, based on the Brillouin zone sampling framework (Chadi, D. J., Cohen, M. L. (1973), Monkhorst, H. L., Pack, J. D. (1976)).

Following the optimisation of the structure, uniaxial strain was employed. The unit cell parameter was subjected to a strain of 1% in each iteration. In the MoS_2 structure, the vertical strain is neglected (Mortazavi, B., Rahaman, O., Dianat, A. & and Rabczuk, T. (2016), Şahin, H., et al. (2009)). Subsequently, the atom positions were recalculated for each step of straining (1%). Following the application of the strain conditions, the optimised geometry was performed using conjugate gradient energy, with the energy convergence criterion set at 10E-5. Finally, strain result calculations were taken for MoS_2 in the optimised +%9, +%12 and -%15 strained geometries.

Results and Discussions

The initial focus is on the optimised lattice parameter. Subsequent to ascertaining the optimal lattice parameter, the total energy values for each lattice parameter were determined by subjecting the lattice parameter to strain in ±3% steps. As demonstrated in Figure 1, the MoS_2 structure exhibits a single minimum in the total energy versus lattice parameter space of the 2D hexagonal Bravais lattice, akin to that observed in C (Graphene) and BN (Boron Nitride). This observation indicates that the MoS_2 structure maintains a planar configuration. In addition to the planar geometry, the MoS_2 structure also exhibits a low-buckled (LB) geometry.

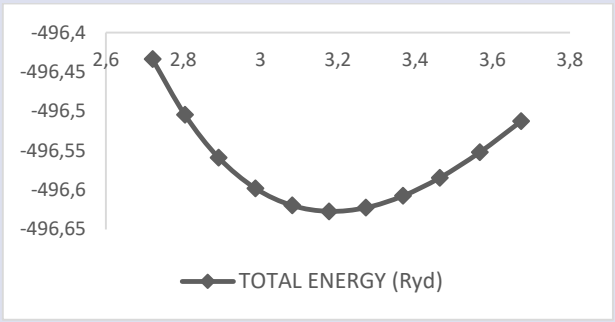

Figure 1. Variation of total energy (Ryd) versus lattice parameter (in Å) of MoS_2 2D- honeycomb structure.

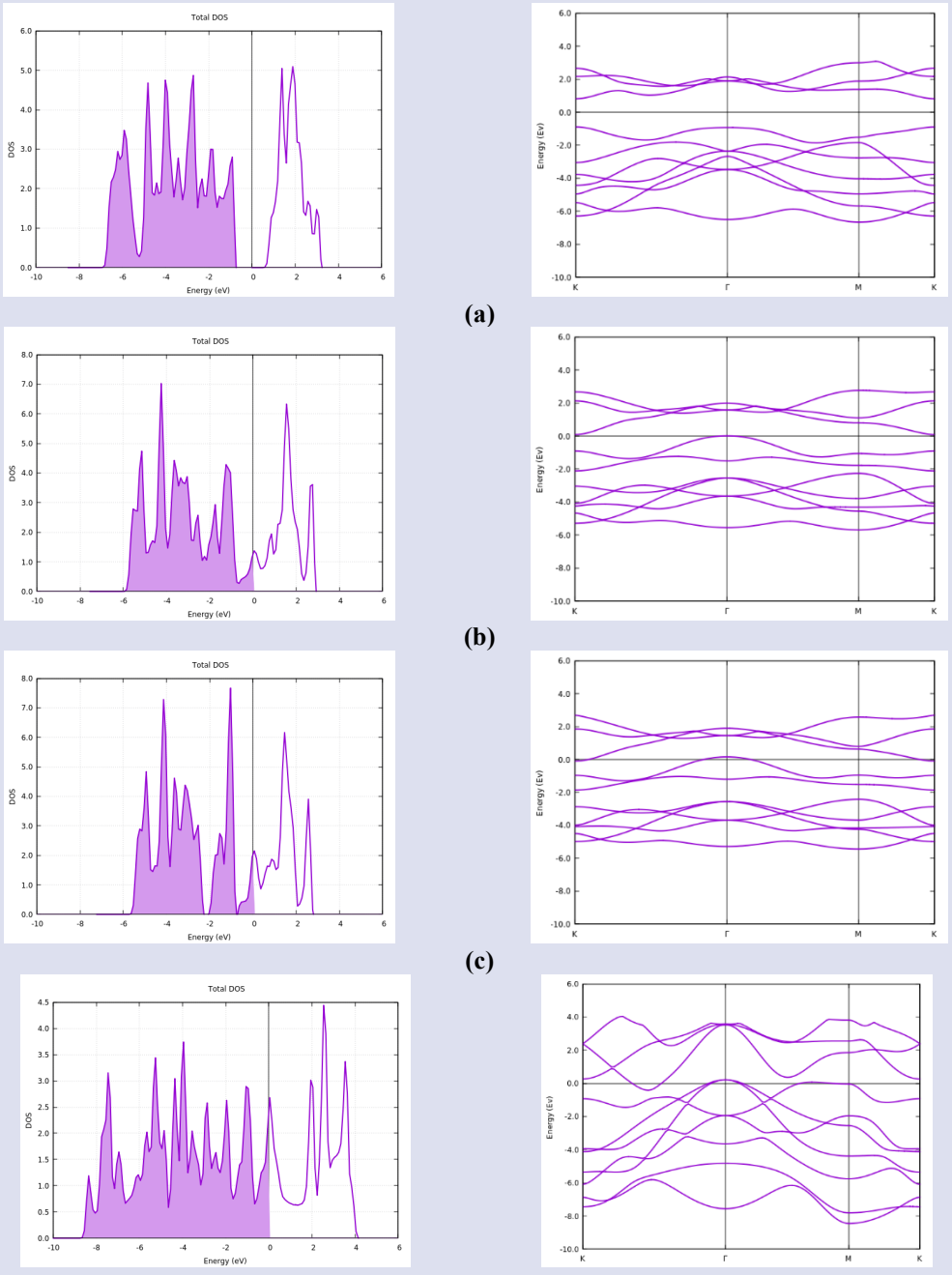

Figure 2. DOS versus energy band graphics for optimised (a), +%9 (b), +%12 (c) and -%15 (d) strained geometries.

In the presence of uniaxial strain, the energy bandgap value decreases with increasing tensile strain. Furthermore, the transition from semiconductor to semi-metal and semi-metal to metal occurs when the uniaxial strain takes higher values (Mortazavi, B., Rahaman, O., Dianat, A. & and Rabczuk, T. (2016)).

Initially, the optimised lattice parameter under strain was calculated by assigning a value less than 0.5 kB, and the Fermi energy value was set to zero in all the graphs drawn, as illustrated in Figure 2(a, b, c, d, e). The optimised geometry a_0 lattice parameter was found to be 3.1771 Å.

In this study, density of states (DOS) and energy versus band graphics using high symmetries points (K, r, M) were plotted by increasing and decreasing the lattice parameter by 1%. Only the graphics of the structure at the transition to the semi-metal and metal structure were included. It was observed that the structure exhibited semi-metallic properties upon compressing the optimised lattice parameter by +%9 (a=3.4630 Å), at which point the VBM and the CBM came into contact with each other at the high symmetry points K and r. Furthermore, the structure demonstrated metallic properties under applied stresses greater than +%9 (a=3.4630 Å), for example +%12 (a=3.5667 Å) and -%15 (a=2.8045 Å). The following text is an excerpt from the aforementioned source:

The process whereby bands at different high-symmetry points interact or interweave is designated as an indirect transition. The article provides a numerical example of the metallic behaviour of MoS_2 in the form of graphs obtained by compressing the lattice parameter +%12 (a=3.5667 Å) and -%15 (a=2.8045 Å).

These results demonstrate that the lattice parameter of the MoS_2 structure transforms firstly into a semi-metal and subsequently into a metal under strains.

3.1. Application of polynomial regression. The generation of a training data set for the valence band minimum and the conduction band maximum is imperative, as the objective is to undertake data mining of the electronic band structure of MoS_2 in the vicinity of the Fermi energy level. It is imperative for the ANN to function effectively. It is noteworthy that the data set under consideration encompasses a substantial number of data sets, numbering in the thousands. However, to date, only 150 data sets have been calculated, based on the number of valence band minimum and conduction band maximum for the optimised geometry, the semi-metallic geometry, the metallic geometry and the insulator geometry.

The PR application for VBM and CBM values is also considered. Initially, the correlation matrix must be examined. This will demonstrate the relationships between the parameters, which are referred to as features in the context of machine learning. A linear relationship between two parameters is indicated by a proximity to unity in the relationship between them. The nature of the relationship between the parameters is longitudinal; however, if the relationship approaches a negative value, the gradient is negative. If the relationship is close to zero, the parameters are still longitudinal, but the gradient of the line will be negative. It is noteworthy that no relationship is observed between the two parameters when the relationship is close to zero.

Figure 3 presents the correlation matrix for MoS_2 for relaxed, +%9, +%12 and -%15 strained geometries.

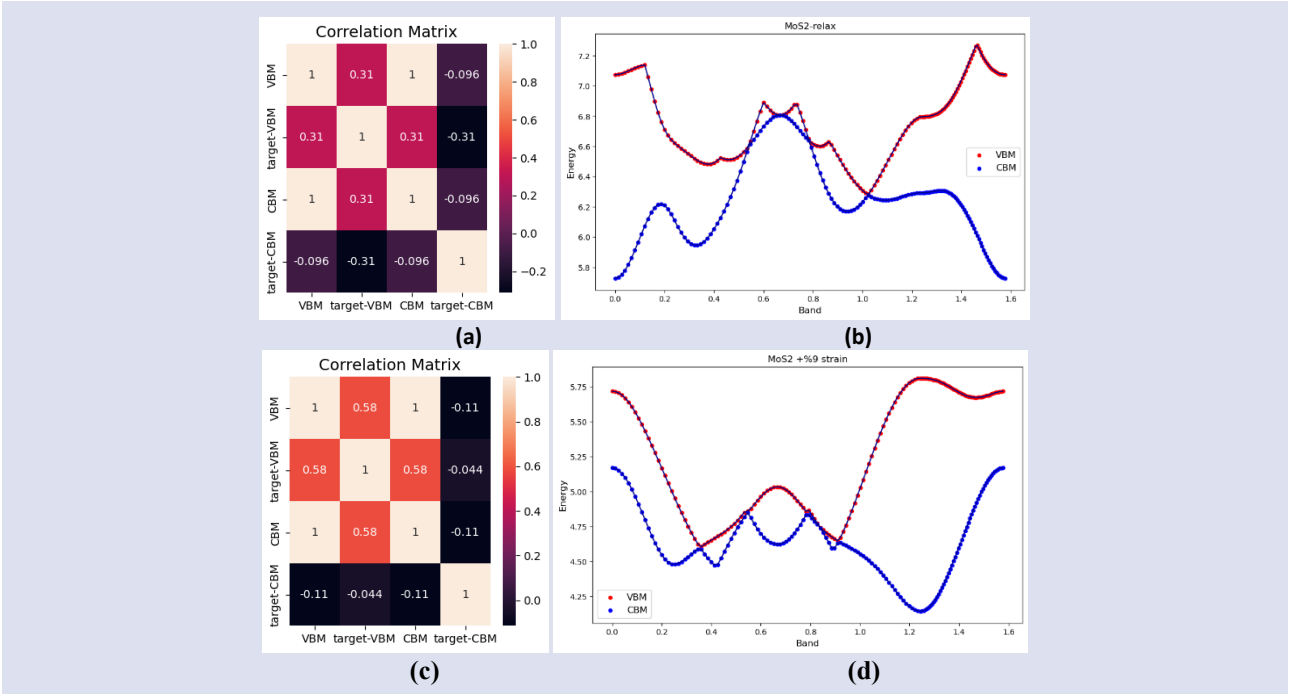

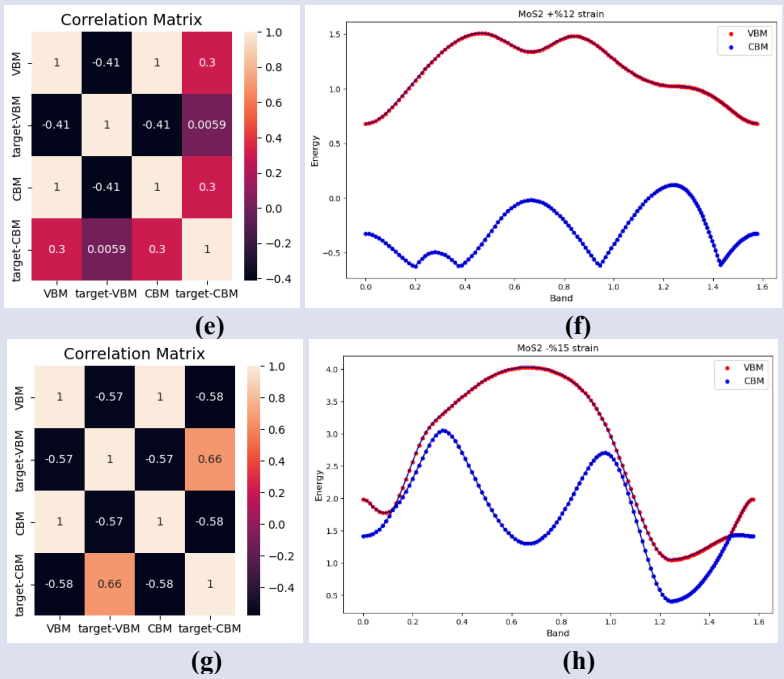

Figure 3. (a), (c), (e), (g) represent the correlation matrix for energy and band values for optimised and +%9, +%12, -%15 strained geometries. (b), (d), (f), (h) represent the behavior of calculated energy versus band values.

The MoS_2 structure demonstrates insulating properties within the optimised geometry. At a straining effect of +9%, the material exhibits semi-metallic properties, while under the same straining effect, it demonstrates metallic properties.

The correlation matrix for each geometry and the energy band graphics are presented in Figure 3. As illustrated in Figure 3(a, c, e, g), the correlations between the energy and band values are 0.31, 0.58, -0.41, -0.58 for VBM values, and -0.096, -0.11, 0.3, 0.41 for CBM values, respectively, for the optimised geometry and +%9, +%12 and -%15 strained geometries, respectively. The use of the minus sign indicates a downward slope, while the plus sign indicates an upward slope. This observation is consistent with the findings depicted in Figure 3(b, d, f, h), which illustrate the curvilinear nature of the results.

The polyfit method, utilised within the numpy module, facilitates the implementation of polynomial regression on the training data. The coefficients and R^2 values corresponding to the optimised and strained geometries are given in Table 1 for VBM and in Table 2 for CBM. The graphs for the optimised and strained geometries are plotted in Figure 4 for CBM and Figure 5 for VBM. The R^2 values are indicative of the model's accuracy. It is evident that as the R^2 values approach one, the consistency of the model is enhanced.

Table 1. The polynomial coefficients for VBM

Polyn. Coeff.	Relaxed Geo.	+%9 Strain	+%12 Strain	-%15 Strain
R^2	0.9814	0.9987	0.9995	0.9993
a_0	7.126	5.696	0.6775	1.433
a_1	-16.21	6.3	0.5411	-4.275
a_2	718.8	-297.2	72.52	162.6
a_3	-1.186E04	4903	72.52	-1294
a_4	1.016E05	-4.523E04	874.6	35.97
a_5	-5.352E05	2.541E05	-1.723E04	7.451E04
a_6	1.879E06	-9.358E06	1.137E05	-5.705E05
a_7	-4.599E06	2.371E07	-4.201E05	2.206E06
a_8	8.06E06	-4.255E06	9.894E05	-5.294E06
a_9	-1.024E07	5.486E06	-1.57E06	8.498E06
a_{10}	9.451E06	-5E093E06	1.718E06	-9.402E06
a_{11}	-6.265E06	3.371E06	-1.303E06	7.209E06
a_{12}	2.905E06	-1.552E06	6.723E05	-3.768E06
a_{13}	-8.Ç938E05	4.716E05	-2.257E05	1.282E06
a_{14}	1.638E05	-8.504E04	4.444E04	-2.562E05
a_{15}	-1.353E04	6892	-3899	2.28E04

Table 2. The polynomial coefficients for CBM

Polyn. Coeff.	Relaxed Geo.	+%9 Strain	+%12 Strain	-%15 Strain
R^2	0.9962	0.9766	0.9766	0.9997
a_0	5.0704	5.176	-0.3389	-2.999
a_1	7.972	-3.337	2.107	-8.507
a_2	-355.2	158.4	-68.69	336.8
a_3	7345	-3744	456	-6513
a_4	-7.2E04	3.842E04	-1609	5.862E04
a_5	4.04E05	-2.274E05	9364	-3.204E05
a_6	-1.484E06	8.742E05	-6.674E04	1.171E06
a_7	3.712E06	-2E311E06	2.931E05	-2.992E06
a_8	-6.592E06	4.358E06	-7.834E05	5.478E06
a_9	8.445E06	-5.833E06	1.356E06	-7.257E06
a_{10}	-7.826E06	5.67E06	-1.578E06	6.957E06
a_{11}	5.194E06	-3.939E06	1.251E06	-4.773E06
a_{12}	-2.405E06	1.906E06	-6.679E05	2.281E06
a_{13}	7.378E05	-6.104E05	2.304E05	-7.209E05
a_{14}	-1.346E05	1.161E05	-4.64E04	1.352E05
a_{15}	1.106E04	-9943	4150	-1.14E04

We can predict new data after obtaining the polynomial coefficients. ANN results are given as the predicted values.

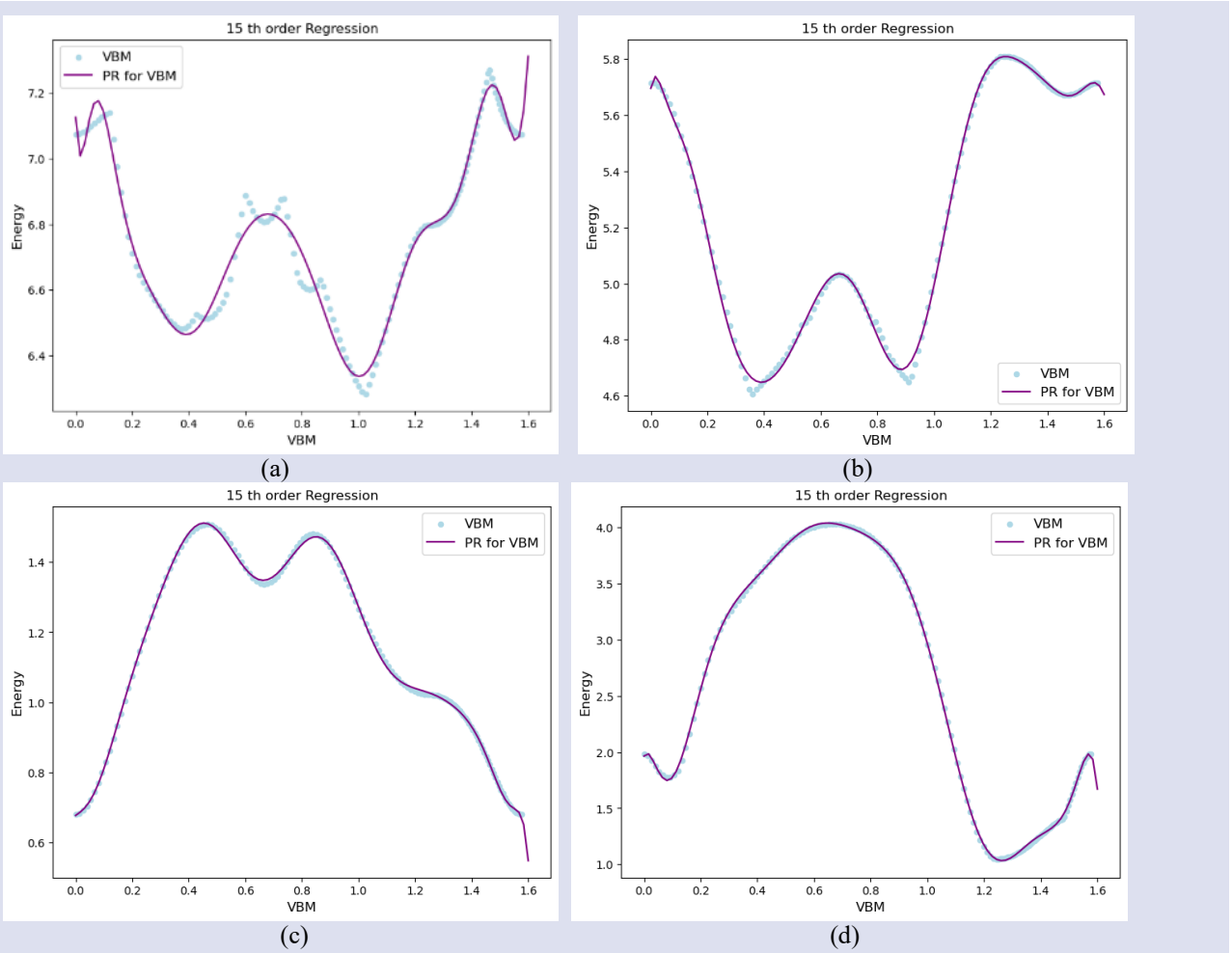

Figure 4. Energy versus band plots for optimised (a), +%9 (b), +%12 (c) and -%15 (d) strained geometries by applying 15th polynomial regression for VBM.

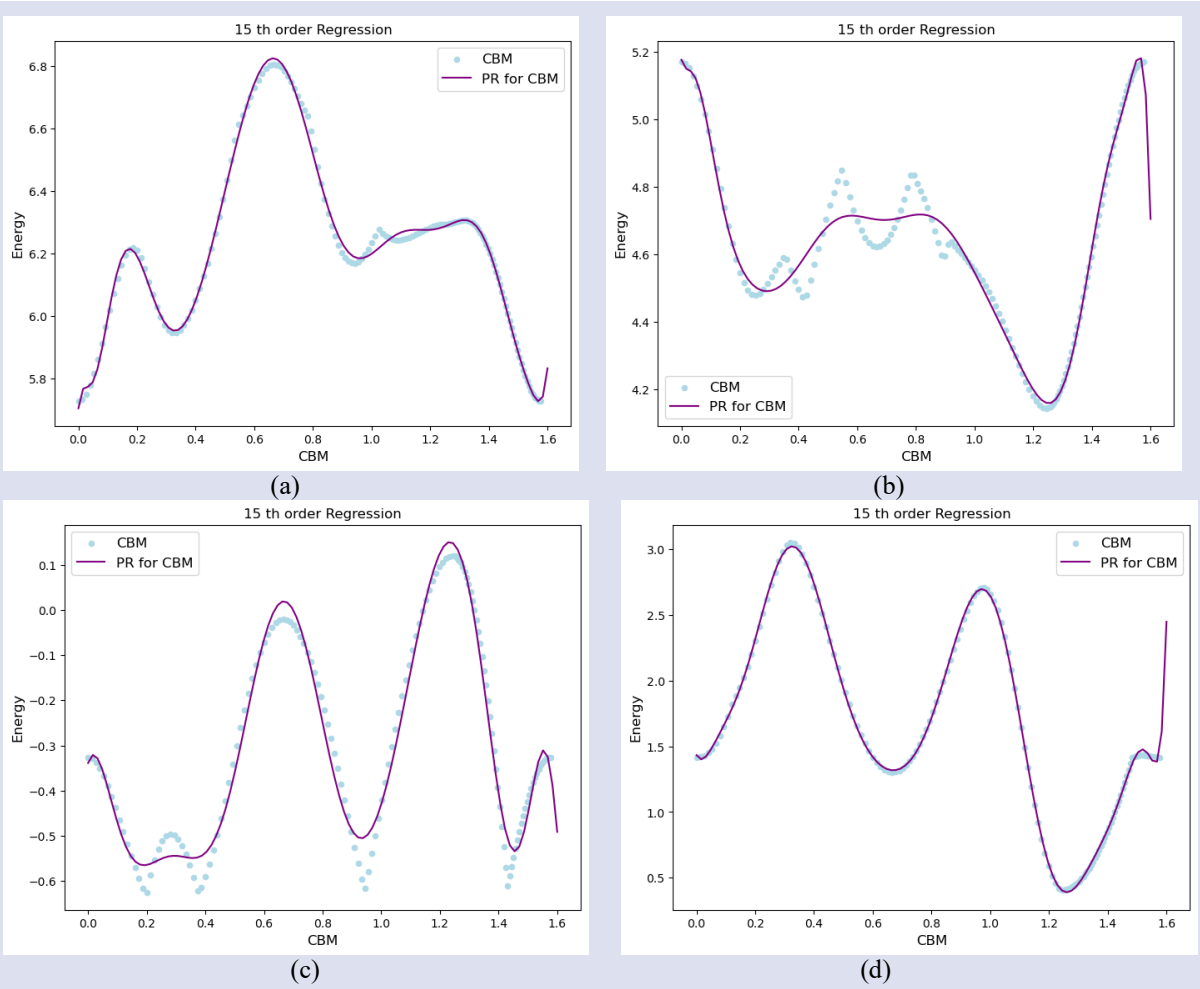

Figure 5. Energy versus band graphics optimised (a), +%9 (b), +%12 (c) and -%15 (d) strained geometries by applying 15th polynomial regression for CBM.

3.2. ANN applications. An application of ANN is different from an application of PR. ANN includes hyperparameters that depend on the type of problem and the user data. Unfortunately, experience and the type of problem determine the values or situations of these hyperparameters. It is important to note that there is no linear relationship between these hyper-parameters. The hyperparameters used for each problem are given in Table 3.

Table 3. The ANN hyperparameters used in this work.

Hyperparameters	Relaxed Geo.	+%9 Strain	+%12 Strain	-%15 Strain
Numbers of neurons	60	40	30	40
Epoch number	900	800	850	900
Batch size parameter	1	1	1	1
Test size	0,3	0,3	0,3	0,3
Validation split number	0,3	0,3	0,3	0,3
Optimizer	adam	adam	adam	adam
Activation function	LRelu	LRelu	LRelu	LRelu

ANN results run Leaky Relu and Elu and 15th order PR results for VBM and their loss plots are shown in Figs. 6 and 7, respectively. ANN and PR results for CBM are shown in Fig. 8 and Fig. 9. To avoid confusion, these figures are shown separately. The results show that PR works well for a wide range of training data. However, the PR results are not satisfactory for the range of out-of-training data. The ANN results are acceptable. ANN performs better than PR on the training data set. In Figure 10, the MoS_2 optimised, semi-metallic and metallic states for VBM and CBM are presented as a single graph for comparison and to make it easier to see the differences.

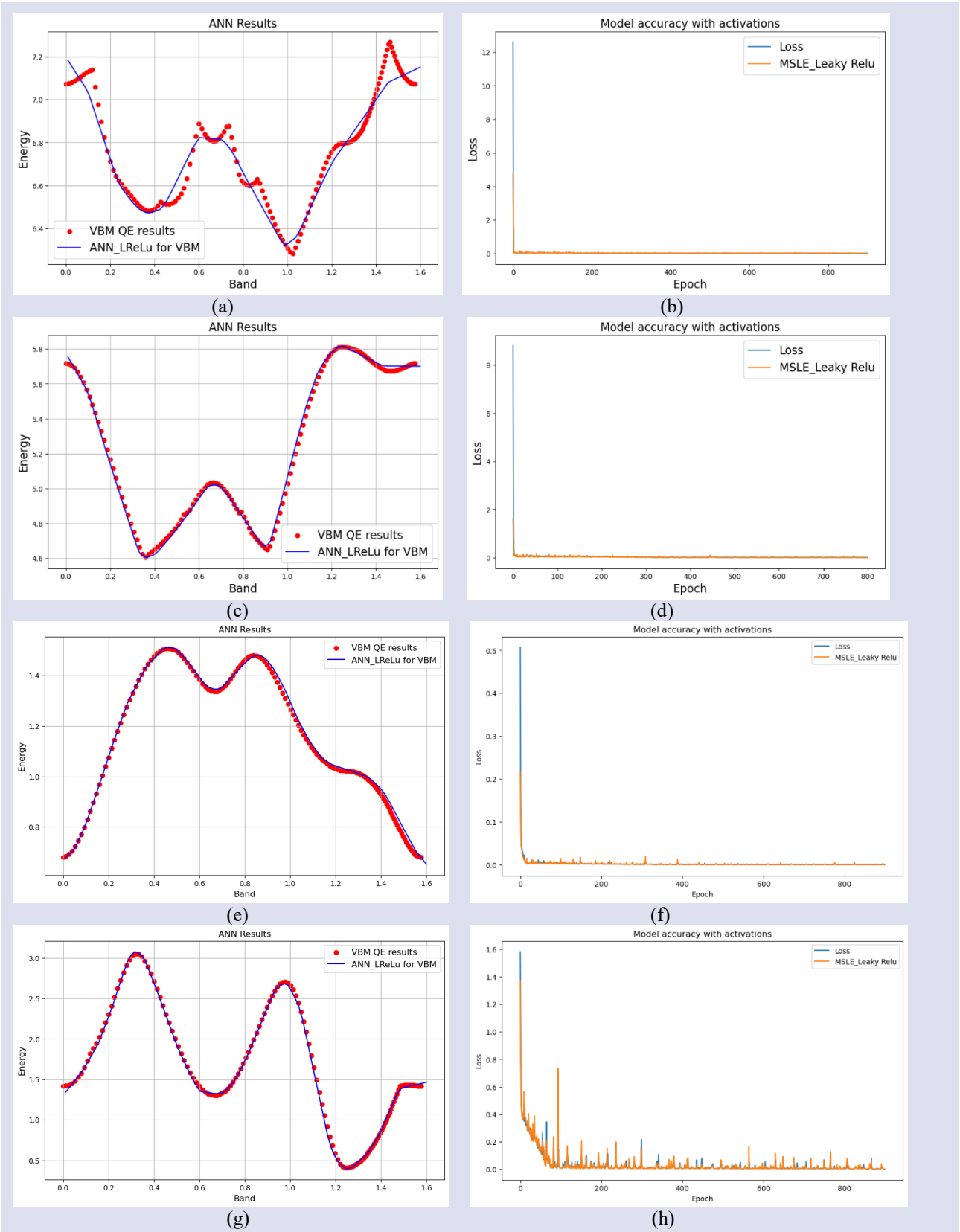

Figure 6. Graphs obtained for the optimised (a, b), +%9 (c, d), +%12 (e, f) and -%15 (g, h) strained geometries and their loss graphs using VBM QE values and Relu.

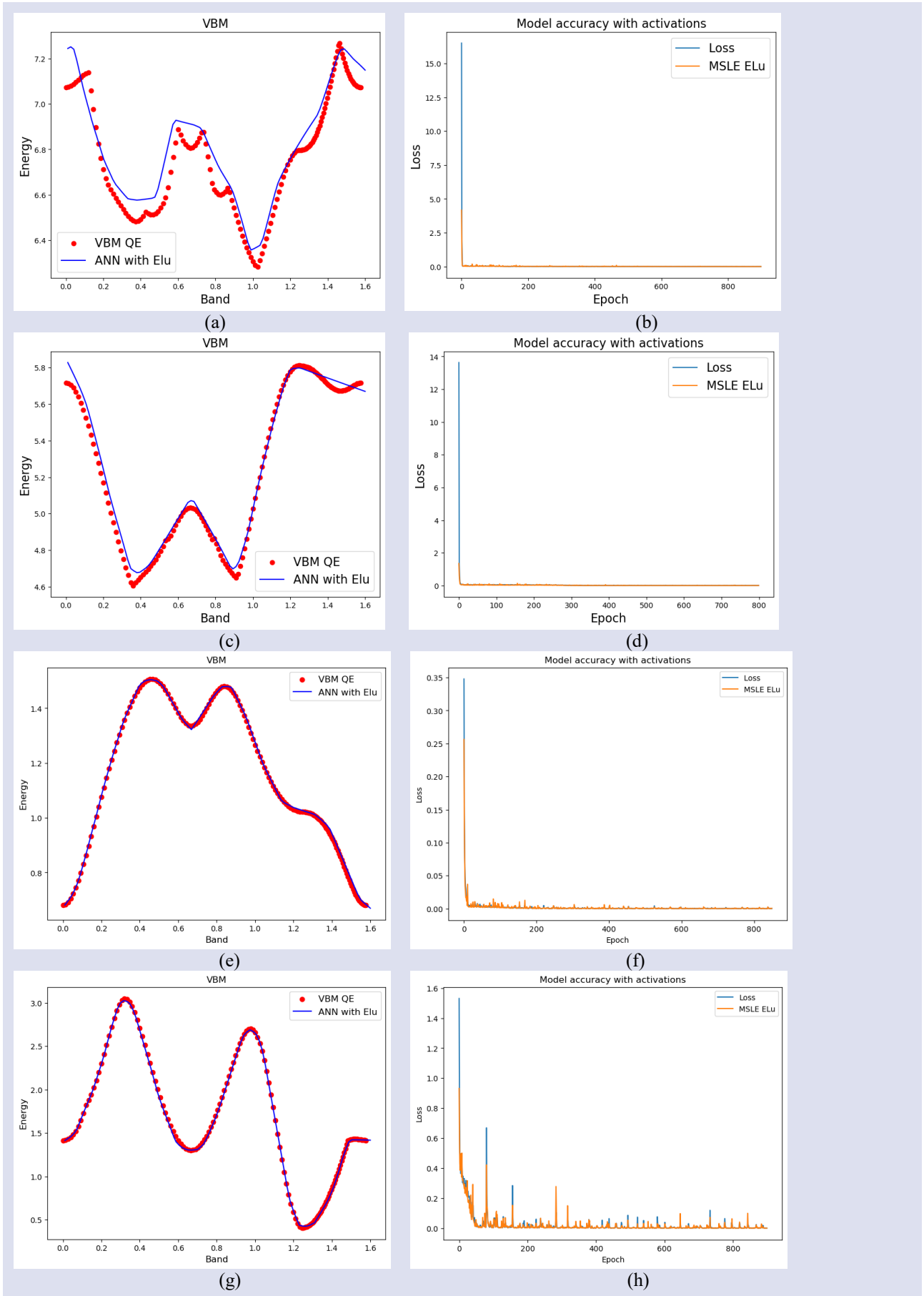

Figure 7. Graphs obtained for the optimised (a, b), +%9 (c, d), +%12 (e, f) and -%15 (g, h) strained geometries and their loss graphs using VBM QE values and Elu.

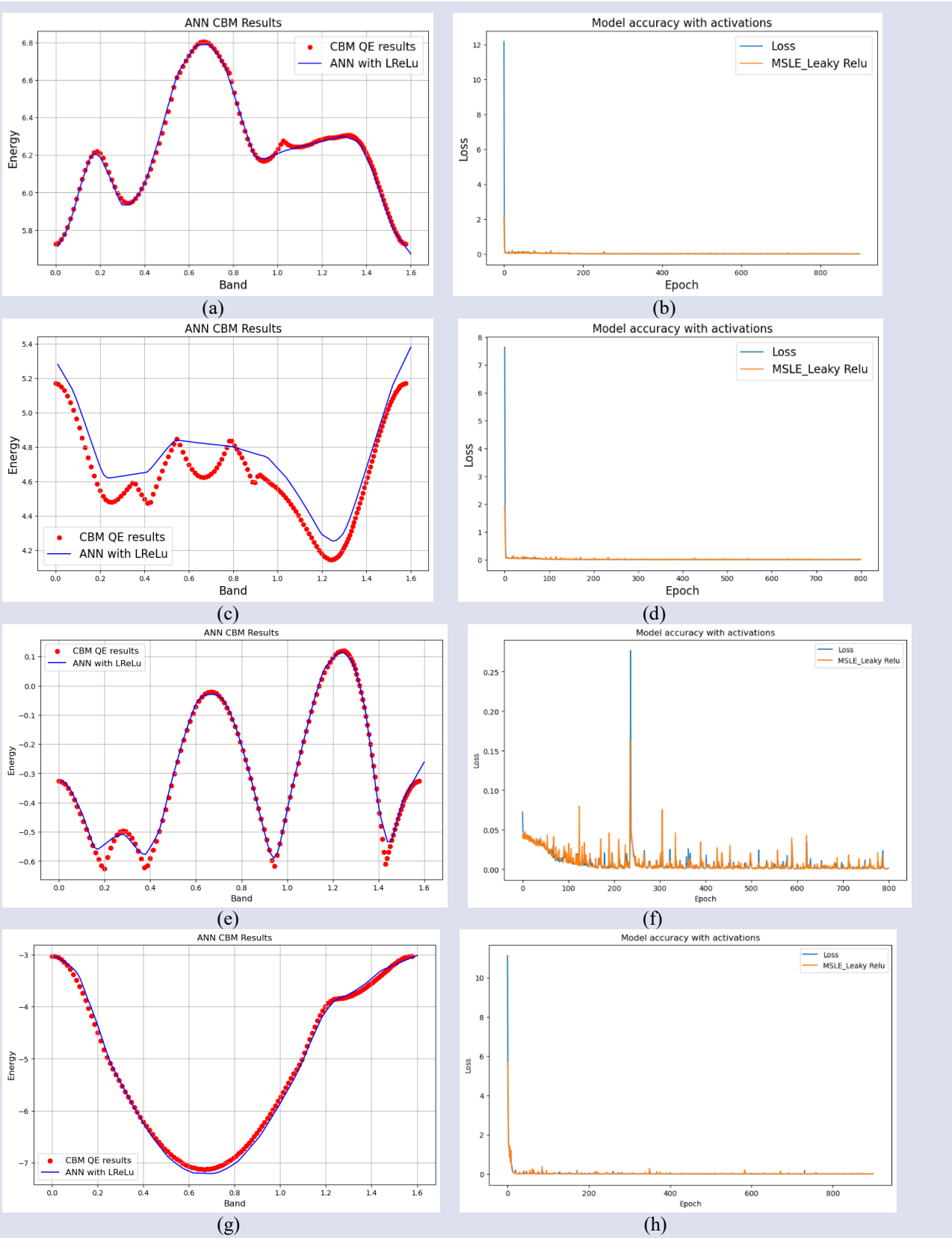

Figure 8. Graphs obtained for the optimised (a, b), +%9 (c, d), +%12 (e, f) and -%15 (g, h) strained geometries and their loss graphs using CBM QE values and Relu.

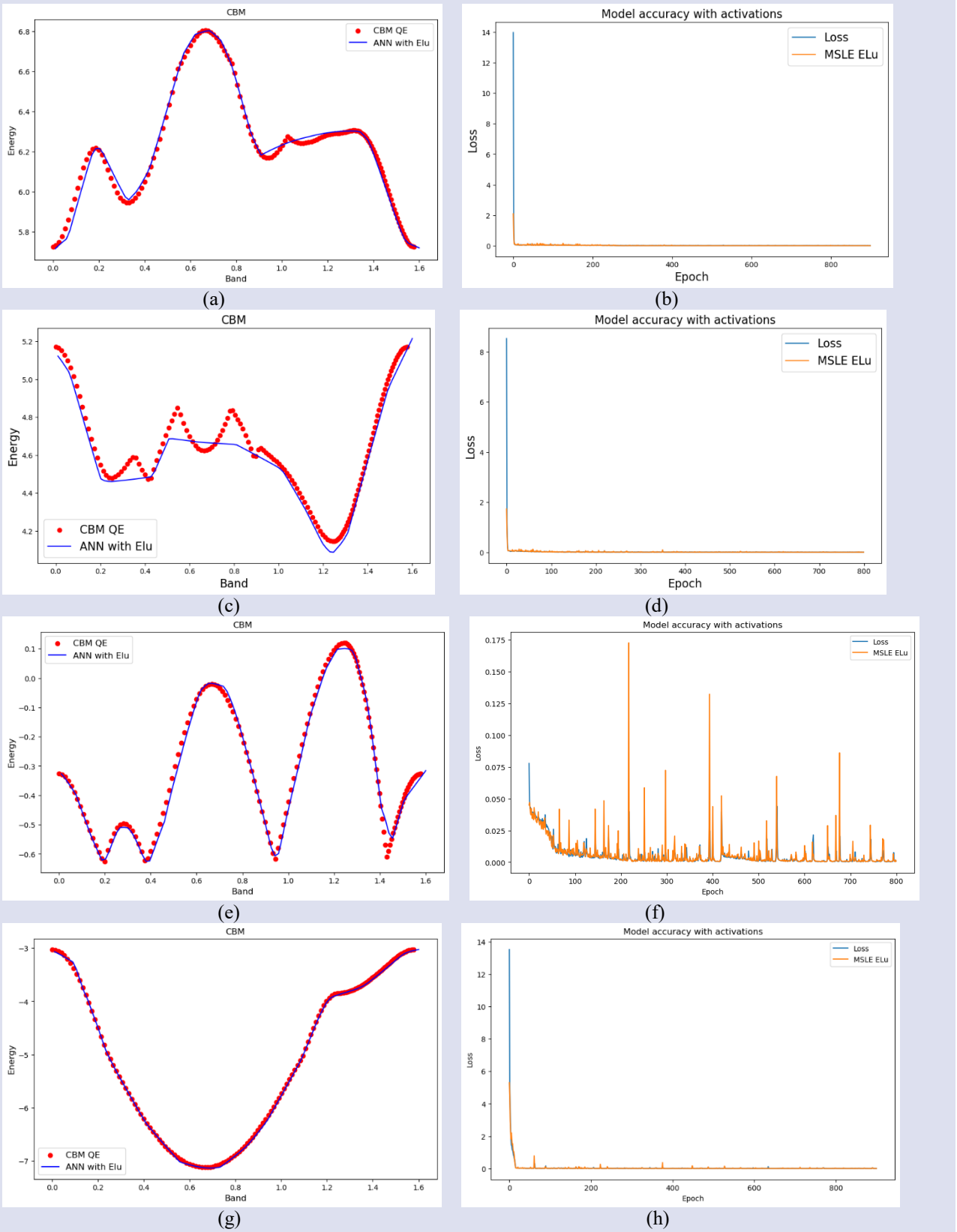

Figure 9. Graphs obtained for the optimised (a, b), +%9 (c, d), +%12 (e, f) and -%15 (g, h) strained geometries and their loss graphs using CBM QE values and Elu.

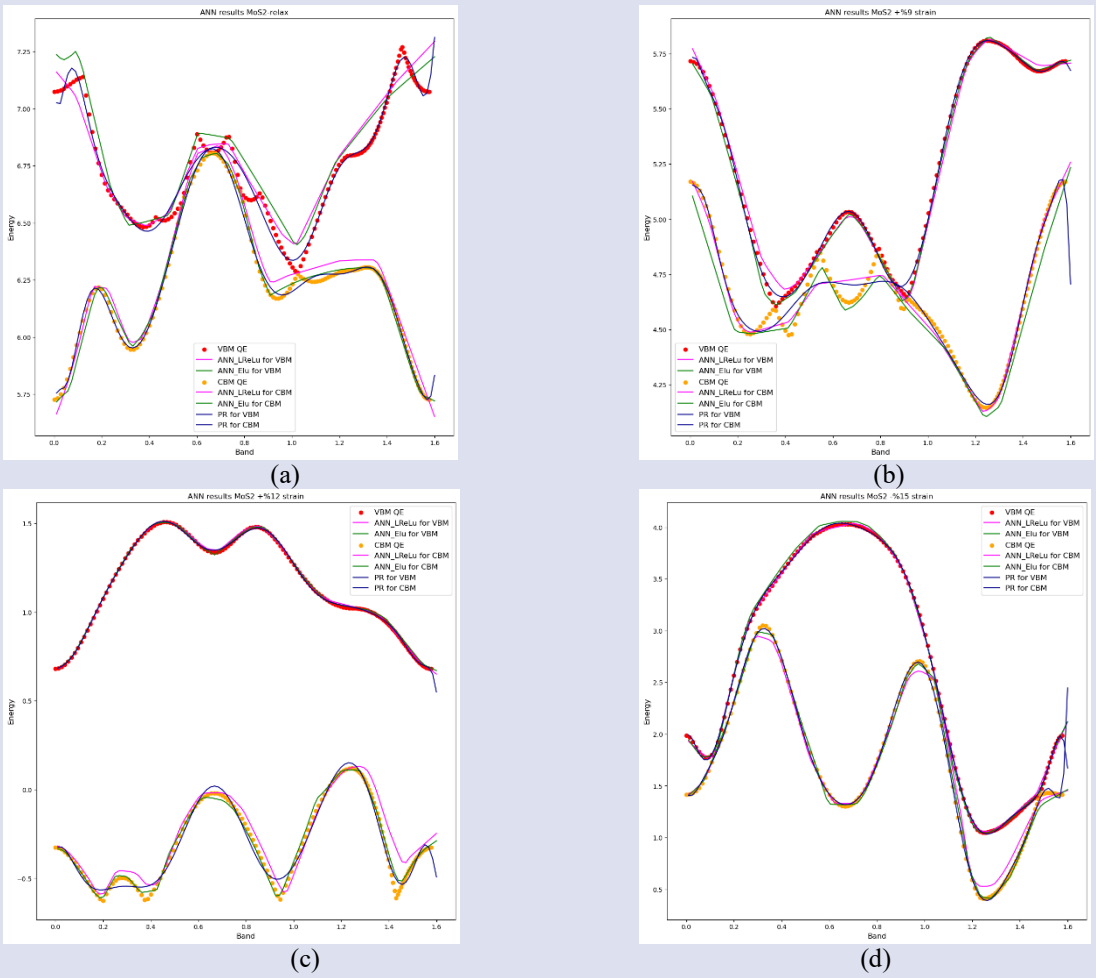

Figure 10. Graphs obtained for the optimised (a), +%9 (b), +%12 (c) and -%15 (d) strained geometries and their loss graphs using CBM and VBM PR values, ANN Elu and LRelu for VBM and CBM.

Conclusions

This study addressed the problem of electronic band transitions in MoS_2 using two different machine learning algorithms, namely PR and ANN. The findings revealed that the MoS_2 structure manifests semi-metallic properties under specific values of the lattice parameter when subject to strain, and metallic properties when the value of this parameter is increased or decreased. An indirect transition, in which the material exhibits half-metallic properties, was observed at the high symmetry points of K and Γ. The present study focuses on the analysis of the VBM and CBM data. The subsequent analysis employs data obtained through the utilisation of the UYBHM. These data serve as the foundation for the subsequent analysis.

The findings of this study demonstrate that the efficacy of machine learning applications is contingent on the magnitude of the training data. In this instance, the research has been conducted with a limited amount of data. Specifically, for VBM and CBM, the dataset consists of 150 unique data points.

The findings indicate that PR is only capable of yielding satisfactory outcomes for the specific range of data employed during model training. Beyond this range, PR's performance deteriorates significantly. Consequently, the predictions derived from PR should be constrained to the range of the training data. In contrast, ANN demonstrates a superior performance, both within and outside the range of the training data. Despite the computational expense of ANN, its efficacy in data analysis renders it a valuable tool. ANN incorporates hyperparameters, which are a distinctive feature of this model.

It is evident that a linear relationship between the hyperparameters of an ANN is not applicable. Table 3 provides a comprehensive overview of the hyperparameters employed in this study.

It is evident that by constructing a more extensive neural network comprising 15 hidden layers as opposed to the conventional 15, the performance of the ANN is rendered unsuitable for the context of longitudinal performance. Conversely, an ANN with a reduced number of layers will also produce an inaccurate result. It is important to note that this comparison is valid only for the number of hidden layers. It is possible to make similar comparisons for other hyperparameters, for example the number of neurons, the activation function and the optimiser. For instance, if one were to presume a greater number of neurons to be available, the ANN would consequently yield an erroneous outcome. It is important to note that the hyper-parameters employed in this study remain valid for the specific set of training data that was utilised. However, it is acknowledged that the hyperparameters may be updated if a richer data set is employed.

Conflicts of Interest

The author declares that there is no conflict of interest in this respect.

Acknowledgements

This work was carried out using the infrastructure of the National High Performance Computing Centre of Turkey (UYBHM).

References

Bertolazzi, S., Brivio, J. & Kis, A. (2011). Streching and breaking of ultrathin MoS_2. ACS Nano, 5, 9703-9709. https://doi.org/10.1021/nn203879f.

Chadi, D. J., Cohen, M. L. (1973). Special Points in the Brillouin Zone. Phys. Rev. B, 8, 5747-5753. https://doi.org/10.1103/PhysRevB.8.5747.

Chhowalla, M., et al. (2013). The chemistry of two-dimensional layered transition metal dichalcogenide nanosheets. *Nature Chemistry*, 5(4), 263-275, https://doi.org/10.1038/nchem.1589.

Giannozzi, P., et al. (2009) . QUANTUM ESPRESSO: a modular and open-source software project for quantum simulations of materials. J. Phys: Condens. Matter, 21, 395502, 1-19. https://doi.org/10.1088/0953-8984/21/39/395502.

Giannozzi, P., et al. (2020). Quantum ESPRESSO toward the exascale. J. Chem. Phys., 152, 154105, 1-11. https://doi.org/10.1063/5.0005082.

Kingma, D. P., Ba, J. L. (2017). Adam: A method for Stochastic Optimization. arXiv:1412.6980v9. https://doi.org/10.48550 / arXiv. 1412.6980.

Kresse, G. (1999). From ultrasoft pseudopotentials to the projector augmented-wave method. Phys. Rev. B, 59, 1758-1775. https://doi.org/10.1103/PhysRevB.59.1758.

Monkhorst, H. L., Pack, J. D. (1976). Special points for Brillouin-zone integrations. Phys. Rev. B, 13, 5188-5192. https://doi.org/10.1103/PhysRevB.13.5188.

Mortazavi, B., Rahaman, O., Dianat, A. & and Rabczuk, T. (2016). Mechanical responses of borophene sheeys: a first-principales study. Chem. Phys., 18, 27405-27413. https://doi.org/10.1039/c6cp03828j.

Novoselov,, K. S., *et* al. (2004). Electric Field Effect in Atomically Thin Carbon Films. Science, 306, 666-669. https://doi.org/10.11216/science.1102896.

Perdew, P. J., Burke, K. & Ernzerhof, M. (1996). Generalized Gradient Approximation Made Simple. Phys. Rev. Lett.,77, 3865-3868. https://doi.org/10.1103/PhysRevLett.77.3865.

Splendiani, A., et al. (2010). Emerging photoluminescence in monolayer MoS_2. Nano Letters, 10(4), 1271-1275. https://doi.org/10.1021/nl903868w.

Şahin, H., et al. (2009). Monolayer honeycomb structures of group-IV elements and III-V binary compounds: First-principles calculations. Physical Review B, 80(15), 155453-(1-12). https://doi.org/10.1103/PhysRevB.80.155453.

Türeci, R. G. (2022). Machine Learning Applications to the One-speed Neutron Transport Problems. Cumhuriyet Science Journal, 43, 726-738. https://doi.org/10.17776/csj.1163514.

Wang, Q. H., et al. (2012). Electronics and optoelectronics of two-dimensional transition metal dichalcogenides. Nature Nanotechnology, 7, 699-712. https://doi.org/10.1038/nnano. 2012.193.

Xu, B., et al. (2015). Emprical Evaluation of Reflected Activations in Convolutional Network. arXiv:1505.00853v2. https://doi.org /10.48550/arXiv.1505.00853.

Zhan, Y., et al. (2012). Large-area vapor-phase growth and characterization of MoS_2 atomic layers on a SiO_2 substrate. Small, 8 (7), 966-971, https://doi.org/10.1002/smll.201102654.